Available online at www.sciencedirect.com
SCIENCE DIRECT®
Acta Materialia 54 (2006) 111–118
Acta MATERIALIA
www.actamat-journals.com

Anisotropic constitutive laws for sintering bodies

Rajendra K. Bordia [a,*], Ruzhong Zuo [b], Olivier Guillon [b], Samuel M. Salamone [a], Jürgen Rödel [b]

[a] Department of Materials Science and Engineering, University of Washington, Box 352120, Seattle, WA 98105, United States
[b] Institute of Materials Science, University of Technology, Darmstadt Petersenstr. 23, D-64287 Darmstadt, Germany

Received 7 March 2005; received in revised form 28 July 2005; accepted 23 August 2005
Available online 10 October 2005

Abstract

Material microstructure and properties become anisotropic during the sintering of cofired ceramics, thin films as well as hot pressed powder compounds. The well-known isotropic constitutive laws are no longer able to describe the sintering process in these cases. Experimental evidence of material anisotropy is given in this paper for alumina thin films and hot forged samples. A new transversely isotropic formulation is developed and the constrained sintering of ceramic films and sinter-forging of powder compacts analyzed using this formulation. Finally, comments regarding the expected values of the parameters and experimental techniques to measure them are presented.

Keywords: Sintering; Anisotropy; Thin films; Modeling; Sinter forging; Ceramics

1. Introduction and background

A prediction of the sintering of complex green bodies [1,2] is possible using a continuum mechanics model incorporating sintering stresses and sintering viscosities [3–8]. The isotropic formulation is well developed and significant progress has been made in using this approach to understand a variety of sintering problems including the densification of constrained films, multi-layered systems, composites and pressure assisted densification. Representative experimental and theoretical studies have been reported in [9–20]. However, for cases where either a non-isotropic strain or non-isotropic stress field is applied to the sintering bodies, directional diffusional fluxes lead to elongated pores and as soon as grain growth sets in to elongated grains. Surface diffusion can react to alleviate anisotropy effects by rounding off pores. This phenomenon was already noted by Rahaman and de Jonghe and Mikeska et al. [5,9] and recently clearly demonstrated by Zuo et al. [15]. Specifically, this anisotropy occurs most dramatically for sintering of thin constrained films, co-sintering of multi-layered systems and sinter-forging. Depending on the specific strain state, the constraint leads to either an orthotropic or transversely isotropic symmetry.

Thin films are widely used as protective coatings for mechanical parts or as active layers on a ceramic substrate with defined conductive, resistive, capacitive, magnetic or piezoelectric properties. As they are constrained by a stiff substrate, an in-plane biaxial tensile stress develops during sintering, which retards overall densification and may induce defects [21–23]. In situ measurements of shrinkage are an experimental challenge. Garino and Bowen [24] studied the sintering behaviour of constrained and free films of glass and polycrystalline ceramics. They used a laser reflectance apparatus to follow thickness changes under isothermal conditions. The isotropic viscous model developed by Scherer and Garino [4] fit the experimental data for glass films, but not for the polycrystalline ZnO and Al_2O_3, which sintered at a much slower rate then predicted by the isotropic viscous sintering models. Several explanations for this discrepancy have been proposed (e.g.,

* Corresponding author. Tel.: +1 206 685 8158; fax: +1 206 5433100.
E-mail address: bordia@u.washington.edu (R.K. Bordia).

1359-6454/$30.00
doi:10.1016/j.actamat.2005.08.025

modified grain growth in constrained films) but without any clear evidence. Bang and Lu [25] using the same type of optical displacement system compared the densification kinetics of borosilicate glass + 20% silica films deposited on silicon substrates. They tried to model the experimental data with existing laws but none of the calculated curves gave a satisfactory fit. Thus, densification kinetics of such films cannot be predicted by classical isotropic models for which the microstructure of a constrained film is assumed to be identical to that of a free film. Working with gold spherical particles [26], they found that more pores were left in the constrained films, although grain sizes were nearly identical in both free and constrained cases. Activation energies of densifying processes were determined and showed that the retardation observed in the constrained-sintering films is primarily due to a change in the densification mechanisms (from a faster grain-boundary diffusion to a slower lattice-diffusion). This leads also to a clearly anisotropic microstructure.

A high demand for miniaturization in the electronics industry has led to multi-layer structures in advanced ceramic packages. Low temperature co-fired ceramics (LTCC) are a challenging application combining different types of sintering materials which are fired in one operation [27]. Tzeng and Jean [28] studied the densification kinetics of laminated alumina/borosilicate glass + alumina/alumina sandwich structures (these external alumina films being non-shrinking green layers). Although the densification mechanism seemed to be controlled by viscous-flow in both free and constrained sintering, the available models overestimated the constrained densification rates. Furthermore, it was shown that the microstructure was affected by constrained sintering. In order to reduce defects such as cracks, delamination or warping induced by differential shrinkage rates and to avoid lateral shrinkage of the LTCC ceramic component, an external uniaxial stress can also be applied [29,30]. However, the applied stresses may also induce anisotropy during sintering.

Sinter-forging is a good experimental method to measure the viscous properties of a sintering material and has been extensively used. In this technique, a uniaxial stress is applied during sintering and radial and axial strains are measured as a function of applied stress. However, it has been recently shown that special attention must be paid to the effect of applied uniaxial stress on the microstructure. A continuous load induces anisotropy in the microstructure giving rise to erroneous values of the constitutive parameters [15]. Anisotropy can be minimized by either applying cyclic loads for a very short time [12] or by conducting discontinuous sinter-forging which requires extensive experimental measurements. Gillia et al. [13] applied an intermittent loading to compute the axial viscosity of WC-Co compacts. During the application of the load, the material may become anisotropic, but after removal of the load it recovers its free sintering isotropic structure in a short time. An improved hot forging technique was also developed by Zuo et al. [16], where the sample is allowed to sinter freely to a prescribed density and then loaded. The constitutive parameters are calculated using the radial and axial strains immediately following the application of the load. Using this technique, constitutive properties were measured with high confidence and reproducibility [16]. These results follow all the theoretical constraints on the constitutive parameters. In particular, this technique, for the first time, has provided reliable and reproducible results on the density dependence of the viscous Poisson's ratio for crystalline materials [31].

It is the objective of this publication to quantify the effect of anisotropy and to provide a theoretical framework for the study of anisotropic sintering bodies. The anisotropy may be inherent in the green microstructure (e.g., due to tape casting) or maybe induced during sintering. Of particular interest is the case of constrained sintering of ceramic films, where no in-plane shrinkage occurs. This behaviour is mimicked by a particular type of sinter-forging, where the applied stress is continuously adjusted to yield zero lateral shrinkage in a macroscopic body [20]. In order to address both these problems, a general transversely isotropic formulation for a sintering body is developed.

2. Isotropic constitutive laws

In this section, we present a summary of results for the relevant problems assuming isotropic behaviour. First, consider the simple constrained film geometry shown in Fig. 1. A porous planar film which is infinite in the in-plane dimensions is being sintered on a rigid substrate. Assuming perfect interface (no sliding) at the interface, the compatibility and equilibrium conditions are

$$\dot{\varepsilon}_1 = \dot{\varepsilon}_2 = 0, \tag{1}$$

$$\sigma_1 = \sigma_2 = \sigma^{\infty} \quad \text{and} \quad \sigma_3 = 0, \tag{2}$$

where $\dot{\varepsilon}_i$ and σ_i are the strain rate and the stress, respectively, in the i direction. Eq. (1) is strictly valid only at the interface between the substrate and the film. Thus, the analysis presented below is valid for thin films. Using the isotropic constitutive relations of the type [7]

$$\dot{\varepsilon}_i^{\text{constr.}} = \dot{\varepsilon}_i^{\text{free}} + \left(\frac{1}{E^{\text{p}}}\right)\left[\sigma_i - \nu^{\text{p}}(\sigma_j + \sigma_k)\right], \tag{3}$$

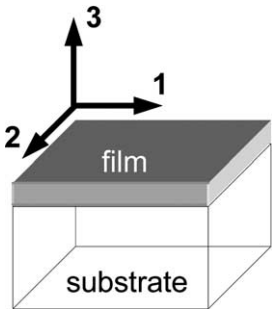

Fig. 1. Schematic of a constrained film geometry and coordinate axis.

where $\dot{\varepsilon}^{\text{free}}$ is the free strain rate due to sintering (that is sintering strain rate in the absence of external or internal stresses), and E^{p} and ν^{p} are, respectively, the uniaxial viscosity and the viscous Poisson's ratio of the porous sintering body. They are functions of the microstructure and evolve during sintering. Using Eqs. (1)–(3), the in-plane stresses and the densification rate of the film can be calculated to be [4]

$$\sigma^{\infty} = -\frac{E^{\text{p}}\dot{\varepsilon}^{\text{free}}}{1-\nu^{\text{p}}}, \tag{4}$$

$$\dot{\varepsilon}_3^{\text{constr.}} = \dot{\varepsilon}^{\text{free}}\left(\frac{1+\nu^{\text{p}}}{1-\nu^{\text{p}}}\right). \tag{5}$$

Note that the in-plane stress, σ^{∞} is tensile (since $\dot{\varepsilon}^{\text{free}}$ is negative, E^{p} is positive, and for isotropic bodies, $0 \leqslant \nu^{\text{p}} \leqslant 0.5$ [6]). In Eq. (5), $\dot{\varepsilon}_3^{\text{constr.}}$ is equal to the volumetric densification rate of the constrained film. The volumetric densification rate for the free film (unconstrained) is $3[\dot{\varepsilon}^{\text{free}}]$. Thus, the relationship between these two quantities is given by

$$\left(\frac{\dot{\rho}}{\rho}\right)^{\text{constr.}} = \frac{1+\nu^{\text{p}}}{(1-\nu^{\text{p}})}\frac{1}{3}\left(\frac{\dot{\rho}}{\rho}\right)^{\text{free}}. \tag{6}$$

It can be seen that the effect of the constraint is to reduce the densification rate of the film (unless $\nu^{\text{p}} = 0.5$) and the magnitude of this reduction depends on the viscous Poisson's ratio, ν^{p}. In Fig. 2, the normalized densification behaviour of the constrained film is schematically shown for different values of ν^{p}. These results are only to illustrate the strong effect of the viscous Poisson's ratio on the densification of constrained films. In a real sintering system, ν^{p} evolves as the microstructure evolves and is affected at least by changes in density [3]. Therefore, comparison between the densification rate of the free and the constrained films should be made for samples with the same density.

Using the isotropic constitutive models, another relevant problem can be analyzed. This problem is to calculate the axial stress needed for zero radial strain rate in a cylindrical sample being sinter-forged under compressive axial stresses [7]. It is given by

$$\sigma_3 = \frac{E^{\text{p}}\dot{\varepsilon}^{\text{free}}}{\nu^{\text{p}}}. \tag{7}$$

This result can also be equivalently written in terms of the sintering potential, Σ [7] as

$$\sigma_3 = \frac{\Sigma(1-2\nu^{\text{p}})}{\nu^{\text{p}}}. \tag{8}$$

Note that the calculated stress is compressive due to the constraints on the value of ν^{p} and because the free sintering strain rate and the sintering potentials are negative. Using this value of the axial stress, the axial strain rate can be calculated to be

$$\dot{\varepsilon}_3 = \frac{1+\nu^{\text{p}}}{\nu^{\text{p}}}\dot{\varepsilon}^{\text{free}}. \tag{9}$$

It should be noted that there is an equivalence between these two problems. The equivalence is in terms of the radial (or in-plane) displacement. In both these problems, the displacement rate in the plane normal to the axial direction is zero. In sintering, the microstructure of the body evolves as it sinters. Assuming negligible neck coarsening (a reasonable assumption in the intermediate and final stages of sintering), it can be postulated that the microstructural evolution is most significantly dependent on the strain state of the body. Thus, although different stress states are used to achieve zero in-plane strain in the two problems, it is expected that the trajectory of microstructural evolution will be similar in these two cases.

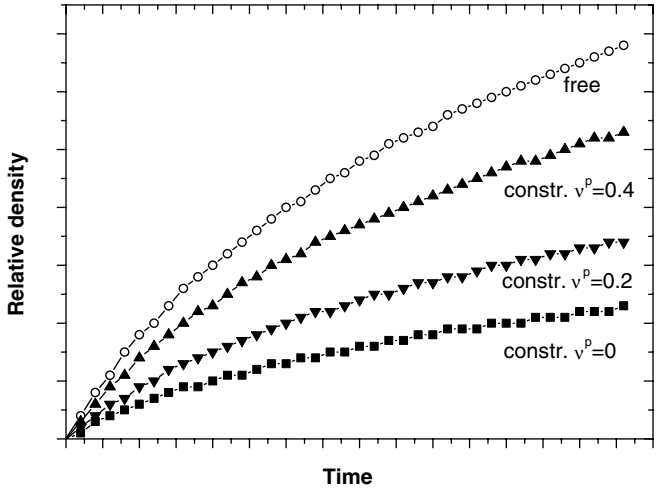

Fig. 2. Effect of Poisson's ratio on the theoretical densification behaviour of constrained isotropic films (schematic representation).

3. Experimental evidence of anisotropy

In this section, we present experimental results on the sintering of constrained films and sinter forged samples, and compare them to the predicted behaviour assuming isotropic constitutive parameters.

3.1. Constrained densification of alumina films

In this study, an ultrafine alumina powder (TM-DAR, Taimei Chemical, Tokyo Japan) was used (particle size 150 nm). Samples for both free and constrained sintering were made from an electrostatically dispersed aqueous slurry containing 40 vol.% solids. The pH of this slurry was adjusted to 3.7 (with nitric acid) and 2 wt.% Carbowax™ 8000 binder (Carbowax Sentry, 8000 Powder NF, FCC grade) was added to provide sufficient green strength to the samples. The samples for free sintering experiments were made by slip casting in a gypsum mold and the constrained film samples were made by sedimentation of powder from this slurry on single crystal sapphire substrates. The cast samples were approximately 6×6 mm cylinders and the films were 6 mm in diameter and $\approx$50 μm thick. The cast samples were dried at room temperature for

24 h followed by drying at 50 °C for 24 h. The green density of the samples was measured to be ≈50%. The densification studies were conducted in a contact dilatometer (Netzsch DIL 402C). The samples were heated to 1050 °C at 10 °C/min followed by a 30 min hold to equilibrate the temperature in the dilatometer. Previous studies have shown that there is negligible densification at this temperature for these powders [32]. Samples were then rapidly heated at 20 °C/min to the sintering temperature between 1200 and 1300 °C and this temperature was held within 2 °C of the isothermal temperature for 5 h.

In Fig. 3, the density as a function of time for both the free sintered and the constrained film densified at 1250 °C is plotted. For this curve, the density at any time was calculated by knowing the final density and back calculating the density at any time from the dilatometer data. It was confirmed that the free sintered sample had isotropic shrinkage (difference between the final shrinkage in the axial and radial direction was less than 1% of the total shrinkage for all temperatures) and the constrained film only shrank in the axial direction (thickness direction). At least two samples were run at each temperature and the presented results are the average of the two samples. In order to improve the accuracy and reproducibility of the measured shrinkage, a dilatometric run with a fully dense alumina of the same thickness as the film was run under the same thermal cycle and this curve was subtracted from the densification run. From repeated measurements, we estimate that the error in the shrinkage measurements is less than 2%.

It is clear from these results that the free samples sintered to almost full density while the constrained samples had significantly retarded densification. In the same figure, the calculated density vs. time for the constrained film is plotted. This was obtained by numerically integrating the calculated constrained densification rate obtained from Eq. (6) using a function for v^{P} from Venkatachari and Raj [11]. It was shown in [31] that this model fits accurately the experimental data measured using discontinuous sinter-forging in a set-up that measured both longitudinal and radial strains. The experiments in [31] were conducted on the same powders as those used in this study. This interrupted technique ensures that the measured properties are for an isotropic microstructure. The simulated curve differs significantly from the experimental one. It significantly overestimates the constrained densification behaviour. As mentioned in Section 2, the analysis is valid for thin films and these films are significantly thicker than the range in which the analysis applies. It is worth mentioning that the constraint is lower for thicker films compared to thin films. Thus it is expected that the fit between the analysis and the experimental results will be even poorer for thin films.

In Fig. 4, the normalized densification rate of the constrained film is plotted as a function of density. In the same figure, the predicted constrained densification rate is also plotted. For this, Eq. (6) together with a dependence of the viscous Poisson's ratio on density from [11] was used. From Fig. 4, it can be seen that the isotropic model overestimates the densification rate of the constrained films by almost a factor of two. Thus, it is clear that the isotropic model is not adequate in predicting the densification behaviour of constrained films. This observation reinforces similar conclusions in [24,28].

3.2. Sinter-forging

For the sinter-forging study, the same alumina powder was used to manufacture green cylinders of 20 mm height and 11 mm diameter (density 58.4%). The samples were first

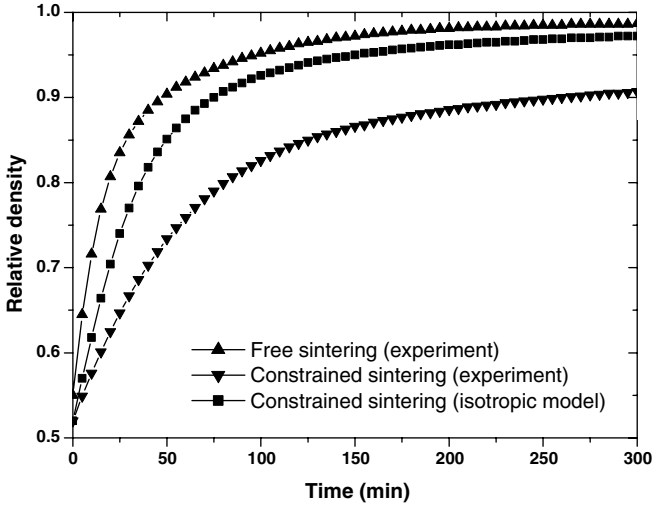

Fig. 3. Comparison between experimental and theoretical densification rates of free and constrained alumina films vs. time (assuming isotropic constitutive laws).

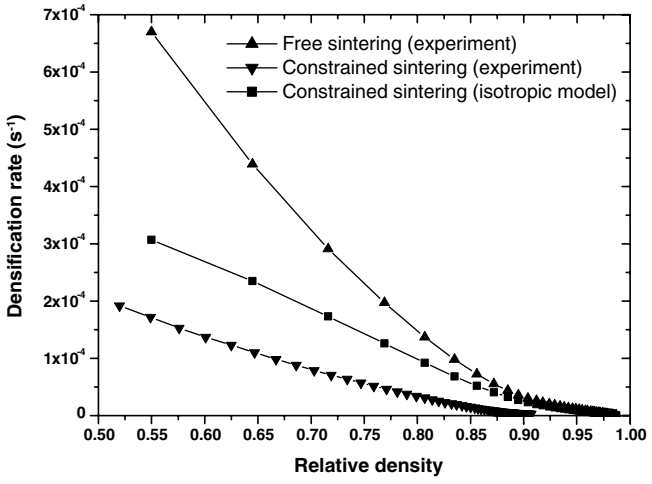

Fig. 4. Comparison between experimental and theoretical densification rates of free and constrained alumina films vs. density (assuming isotropic constitutive laws).

pressed using a uniaxial pressure of 100 MPa and then consolidated by cold isostatic pressing with 250 MPa. Samples were heated at a constant rate of 30 °C/min to 1250 °C. In this study, a compressive uniaxial load was applied to inhibit radial shrinkage. The value of the load was continuously regulated to achieve zero radial strain rate. It remains between −20 and −30 MPa during the intermediate stage of sintering and decreases to zero for densities above 0.95. Using Eq. (7) with experimentally determined values of uniaxial viscosity E^{p} (from [16] in which the same alumina powders as those used in this study) and Poisson's ratio v^{p} (from [11]) it is possible to compute the theoretical uniaxial compressive stress needed for zero radial shrinkage (Fig. 5). Although the trends are quite similar between the two curves, it is obvious that the absolute value of the predicted stress is lower than the experimental one by a factor of 3.

From both sets of experiments, it is apparent that the isotropic constitutive models are inadequate in predicting the observed experimental results. It should be noted that the required constitutive parameters for this comparison have been obtained with well-controlled experiments. Thus, the conclusion from these observations is that the basic assumptions of the model are not correct. The key assumption for the validity of the isotropic model is that the microstructure for the constrained film and the sinter-forged sample is identical to the microstructure at the same density for a freely sintering sample [5]. In particular, the samples must have the same grain and pore size, shape and orientation. We have clearly shown that this is not the case for the sinter-forged and free sintered samples [15]. By carefully examining the microstructure in high resolution SEM and quantifying the pore orientation (polar plots), it was shown that the pores are randomly oriented in the free sintered samples but had preferential orientation (see Fig. 4 in [15]). An applied compressive stress promotes densification, and neck growth in the plane perpendicular to its direction. During free sintering, spherical pores remain spherical as densification is isotropic (Fig. 6). Under uniaxial stress pores have a non-spherical geometry (like an ellipsoid) with the orientation as shown in Fig. 6. Due to this induced anisometry, it is expected that the constitutive properties of the compact will become anisotropic. For example, the densification rate is proportional to the sintering stress Σ, which is dependent on the inverse of the radius of curvature of the pores. Since the pore radii are anisometric, the free densification rate is expected to be anisotropic. Similarly, the uniaxial viscosity, E^{p}, which is a strong function of contact area, will be anisotropic.

From the experimental results on zero radial strain rate sinter-forged samples, there is clear and direct evidence of anisotropic microstructure evolution. Although, there is no direct evidence of anisotropic microstructure in the constrained films, based on the equivalent strains in the constrained films and the zero-radial strain rate sinter-forged samples, it is postulated that this microstructure will also be transversely isotropic.

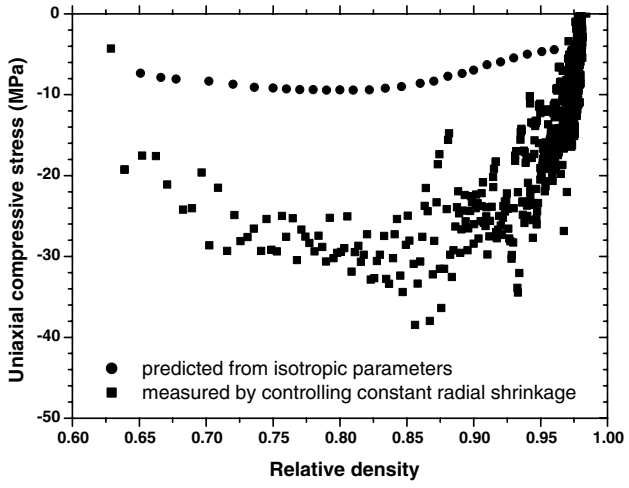

Fig. 5. Measured and predicted (using isotropic formulation) compressive stresses for zero-radial strain.

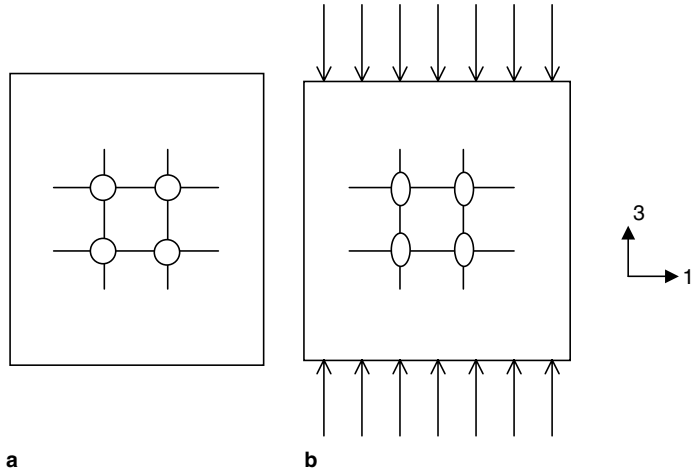

Fig. 6. Schematic of pore structure in free sintered (a) and hot forged (b) specimens.

4. Anisotropic model for constrained sintering and sinter-forging

From the previous section, it is clear that during sinter forging, the microstructure becomes anisotropic and there is a deformation equivalence between constrained sintering and zero-radial stain rate sinter-forging (in both cases the displacement rate in one plane is zero). We, therefore, postulate that the microstructure of constrained sintering films becomes anisotropic. We also propose that this microstructural anisotropy is the reason why the isotropic constitutive models are inadequate in predicting the densification behaviour of constrained films. The anisotropy is such that the microstructure in the plane of the film (1–2 plane in Fig. 1) is isotropic. Thus, it is a case of a transversely isotropic body. In this section, we develop a transversely isotropic formulation for a sintering body and apply this to constrained film sintering and to sinter-forging.

For an orthotropic body undergoing viscous deformation with densification, the constitutive relations in terms of the principle stress and strain can be written as

$$\dot{\varepsilon}_1 = \dot{\varepsilon}_1^{\text{free}} + \frac{\sigma_1}{E_1^{\text{p}}} - \frac{\nu_{21}^{\text{p}}\sigma_2}{E_2^{\text{p}}} - \frac{\nu_{31}^{\text{p}}\sigma_3}{E_3^{\text{p}}}, \tag{10a}$$

$$\dot{\varepsilon}_2 = \dot{\varepsilon}_2^{\text{free}} + \frac{\sigma_2}{E_2^{\text{p}}} - \frac{\nu_{12}^{\text{p}}\sigma_1}{E_1^{\text{p}}} - \frac{\nu_{32}^{\text{p}}\sigma_3}{E_3^{\text{p}}}, \tag{10b}$$

$$\dot{\varepsilon}_3 = \dot{\varepsilon}_3^{\text{free}} + \frac{\sigma_3}{E_3^{\text{p}}} - \frac{\nu_{23}^{\text{p}}\sigma_2}{E_2^{\text{p}}} - \frac{\nu_{13}^{\text{p}}\sigma_1}{E_1^{\text{p}}}. \tag{10c}$$

For the special case of a transversely isotropic body with the 1–2 plane being the isotropic plane, the properties in plane are the same. As a result

$$\dot{\varepsilon}_1^{\text{free}} = \dot{\varepsilon}_2^{\text{free}}, \tag{11a}$$

$$E_1^{\text{p}} = E_2^{\text{p}}, \tag{11b}$$

$$\nu_{12}^{\text{p}} = \nu_{21}^{\text{p}}, \tag{11c}$$

$$\nu_{31}^{\text{p}} = \nu_{32}^{\text{p}}, \tag{11d}$$

$$\nu_{23}^{\text{p}} = \nu_{13}^{\text{p}} \tag{11e}$$

and thus Eq. (10) reduces to

$$\dot{\varepsilon}_1 = \dot{\varepsilon}_2 = \dot{\varepsilon}_1^{\text{free}} + \frac{1}{E_1^{\text{p}}}\left(\sigma_1 - \nu_{12}^{\text{p}}\sigma_2 - \frac{E_1^{\text{p}}}{E_3^{\text{p}}}\nu_{31}^{\text{p}}\sigma_3\right), \tag{12a}$$

$$\dot{\varepsilon}_3 = \dot{\varepsilon}_3^{\text{free}} + \frac{1}{E_3^{\text{p}}}\left(\sigma_3 - \nu_{13}^{\text{p}}\frac{E_3^{\text{p}}}{E_1^{\text{p}}}(\sigma_1 + \sigma_2)\right). \tag{12b}$$

4.1. Constrained Film

Consider again the geometry shown in Fig. 1. Since the in-plane deformation is constrained and the out of plane is not, it is expected that the sample will become transversely isotropic. It will be isotropic in the plane of the film (1–2 plane) but the microstructure in this plane will be different than that in the 1–3 plane since the film can only shrink in the thickness (i.e., 3) direction. Using the compatibility and equilibrium conditions, Eqs. (1) and (2), and the transversely isotropic constitutive relations (Eq. (12)), we obtain the following expressions for the in-plane stress σ^{∞} and the constrained densification rate of the film $\dot{\varepsilon}_3^{\text{constr.}}$:

$$\sigma^{\infty} = -\frac{E_1^{\text{p}}\dot{\varepsilon}_1^{\text{free}}}{1-\nu_{12}^{\text{p}}}, \tag{13}$$

$$\dot{\varepsilon}_3^{\text{constr.}} = \dot{\varepsilon}_3^{\text{free}} + \frac{2\nu_{13}^{\text{p}}}{1-\nu_{12}^{\text{p}}}\dot{\varepsilon}_1^{\text{free}}. \tag{14}$$

As can be seen, these relations are similar to the isotropic case (Eqs. (4) and (5)). The appropriate anisotropic viscosities and viscous Poisson's ratio are needed. In addition, instead of one free strain rate, we need two free strain rates due to the anisotropic nature of the microstructure.

The constrained densification rate is however no longer directly linked to the free densification rate. It depends now on the Poisson's coefficient ratio and additionally on the free strain rate in direction 3

$$\left(\frac{\dot{\rho}}{\rho}\right)^{\text{constr.}} = \frac{\nu_{13}^{\text{p}}}{1-\nu_{12}^{\text{p}}}\left[\left(\frac{\dot{\rho}}{\rho}\right)^{\text{free}} + \dot{\varepsilon}_3^{\text{free}}\right] - \dot{\varepsilon}_3^{\text{free}}. \tag{15}$$

4.2. Sinter-forging

The stress state for a body being sinter-forged (assuming no friction at the platens) is $\sigma_1 = \sigma_2 = 0$ and $\sigma_3 \neq 0$. For this case, Eq. (12) reduces to

$$\dot{\varepsilon}_1 = \dot{\varepsilon}_2 = \dot{\varepsilon}_1^{\text{free}} - \frac{\nu_{31}^{\text{p}}\sigma_3}{E_3^{\text{p}}}, \tag{16a}$$

$$\dot{\varepsilon}_3 = \dot{\varepsilon}_3^{\text{free}} + \frac{\sigma_3}{E_3^{\text{p}}}. \tag{16b}$$

Applying Eq. (16) to the special case of zero radial strain rate sinter-forging, we obtain that the axial stress needed for achieving a zero radial strain rate is

$$\sigma_3 = \frac{E_3^{\text{p}}\dot{\varepsilon}_1^{\text{free}}}{\nu_{31}^{\text{p}}} \tag{17}$$

and the corresponding axial strain rate is given by

$$\dot{\varepsilon}_3 = \dot{\varepsilon}_3^{\text{free}} + \frac{1}{\nu_{31}^{\text{p}}}\dot{\varepsilon}_1^{\text{free}}. \tag{18}$$

Eqs. (17) and (18) are modified versions of the stress and strain rate calculated for the isotropic case (Eqs. (7) and (9)).

5. Transversely isotropic constitutive parameters

According to the transversely isotropic formulation developed in the last section, five independent viscous constitutive parameters and two free sintering strain rates are needed as a function of microstructure to fully describe the behaviour of sintering bodies. It should be noted that for transversely isotropic viscous bodies, all five of the constitutive parameters are independent. This should be contrasted to the case of the transversely isotropic elastic

body for which only four parameters are independent. The reason for this difference is that for an elastic body, the thermodynamic requirement that the strain energy is a state variable (path independent) leads to an additional relationship between elastic constitutive parameters. For a viscous body, there is no such requirement between constitutive parameters. The transversely isotropic case should be contrasted with the case of sintering of isotropic bodies for which only two constitutive parameters and one free strain rate are required. For specific problems, fewer parameters maybe required. For example, only four parameters are needed to obtain the strain rate of a constrained thin film (Eq. (14)). These are: $\dot{\varepsilon}_1^{\text{free}}$, $\dot{\varepsilon}_3^{\text{free}}$, v_{21}^{p}, v_{13}^{p}. Physically, the viscosities govern the effect of stress on the strain in the same direction and the viscous Poisson's ratios give the effect of stress to the strain in orthogonal direction. Thus, for a stress in the i direction

$$E_i^{\text{p}} = \frac{\sigma_i}{\dot{\varepsilon}_i - \dot{\varepsilon}_i^{\text{free}}}, \tag{19a}$$

$$v_{ij}^{\text{p}} = \frac{\dot{\varepsilon}_j^{\text{free}} - \dot{\varepsilon}_j}{\dot{\varepsilon}_i - \dot{\varepsilon}_i^{\text{free}}}. \tag{19b}$$

It should be noted that these parameters are function of the microstructure. This induces an additional level of complexity and requires the development and measurement of appropriate microstructural parameters to quantify both the average and the anisotropic state of the microstructure. An example of this was presented in [15], where it was shown that the orientation of the pores is one measure of the extent of anisotropy in the microstructure. Given this level of complexity, it is important to get a sense of the bounds on the range of the values that should be expected for anisotropic sintering bodies. At one extreme are the isotropic bodies for which now there are reasonable models and experimental values of the constitutive parameters [16,18,19,31,33]. Further experimental work is needed to broaden the range of materials and processing parameters. The experimental results will lead to a refinement of the models which relate the constitutive parameters to the microstructure.

For the transversely isotropic case, at the other end of the isotropic microstructure is the microstructure obtained in the fully constrained film or the zero radial strain rate sinter-forging. Here, we report preliminary results on the first set of zero radial strain rate experiments. Zero radial strain rate sinter forging was conducted on alumina. The experimental details are provided in Section 3.2.

We have used the zero radial strain rate experiments to investigate the limit of anisotropy that can be induced. In these experiments, the axial load was precisely controlled to give a zero radial rate. The load was maintained until the sample densified to a pre-determined density and then the load was removed. After removing the load, the axial and radial strains were monitored. In the terminology of this paper, we have measured $\dot{\varepsilon}_1^{\text{free}}$ and $\dot{\varepsilon}_3^{\text{free}}$ for the most anisotropic microstructure that can be expected. Fig. 7 plots the ratio of radial to axial strain rate as a function of time after removal of the load. It should be noted that soon after the removal of the load, the sample sinters faster in the radial direction compared to the axial direction and over time this ratio decreases. For samples that were sinter-forged to the lowest densities (70% and 75%), this ratio decreases to 1 in about 40 min and the sample behaves as an isotropic material after that time. For samples that were sinter-forged to a higher density and hence are more anisotropic, we observe a higher value of the initial anisotropy which takes longer to be eliminated. In addition, for these samples we observe a reversal at longer times such that the radial strain rate becomes less than the axial strain rate. These results are preliminary and further confirmation of this is needed. It should be noted that this is only observed at long times where both axial and radial rates are low and measurement is more prone to errors.

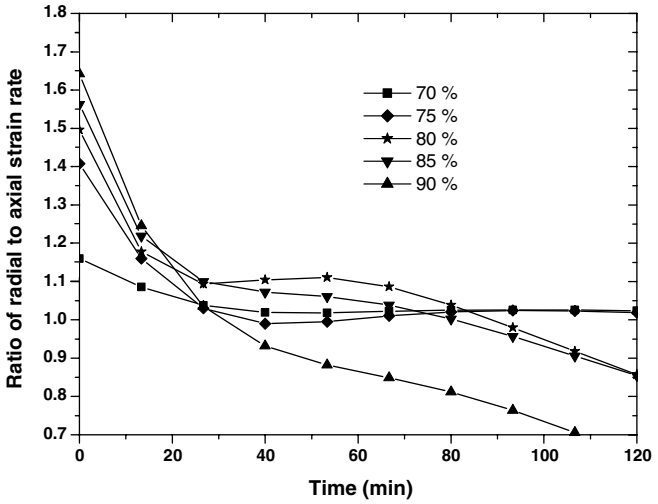

Fig. 7. Experimental radial to axial strain ratio as a function of time after removal of load for different degrees of densification.

The most important result from this study is shown in Fig. 8, where we plot the maximum value of ratio of the radial to axial strain rates as a function of the density to which the sample has been sinter-forged (under conditions of zero radial strain rate). Several important points are illustrated in this figure. First, the ratio of the anisotropy in the free strain rates ranges from about 1.1 to 1.65. This gives a sense of the maximum anisotropy which results during sinter forging under the conditions of zero radial shrinkage. The second important point is that, as expected, the longer the load is maintained, the higher is the anisotropy in the free strain rates. The anisotropy as measured by the free strain rates decreases for high density (greater than 90%). This is to be expected since in the extreme case of a fully dense body, this ratio will be equal to one (both the radial and the axial strain rates would be zero). However, this does not mean that the sample that has been sinter forged to 95% density is less anisotropic than the sample sinter forged to 90%. It is anticipated that measurement of other parameters (e.g., viscosities) will show that the

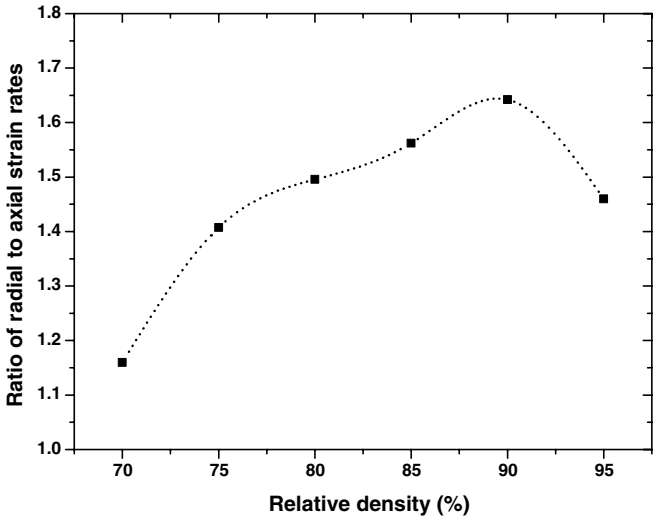

Fig. 8. Experimental radial to axial strain ratio right after the load has been taken off ($t = 0$) as a function of density.

anisotropy continues to increase the longer the sample is sinter forged.

We can now also reconsider the stress required to maintain zero radial strain rate (Fig. 5) and compare the anisotropic case (Eq. (17)) with the anisotropic formulation (Eq. (7)). While the influence of the viscous Poisson's ratio is difficult to analyze, it is apparent that the anisotropy with large necks perpendicular to the axial direction (Fig. 6) will lead to an increase in E_3^{p}. Similarly, an increased $\dot{\varepsilon}_1^{\mathrm{free}}$ (Fig. 8) will require an increased axial stress σ_3 in order to maintain a zero radial strain rate, if comparison of the anisotropic with the isotropic case is contemplated. The result in Fig. 5 can therefore be qualitatively rationalized.

This first study has measured the maximum anisotropy that may be induced in two of the seven parameters (free strain rates in orthogonal directions). Additional experimental studies are underway to get a sense of the extent of anisotropy in the constitutive parameters (viscosities as well as viscous Poisson's ratios).

6. Summary and conclusions

In this paper, we have shown that in some cases, the microstructure of a sintering body becomes anisotropic due to non-hydrostatic stresses during sintering. Two particular cases are considered to highlight this situation: the sintering of constrained films and sinter-forging. It is shown that the well-established isotropic continuum formulation is not adequate to model the experimental observations. A general transversely isotropic viscous formulation is developed for sintering bodies and applied to the specific cases of constrained densification of films and sinter forging. It is shown that for this case, five constitutive parameters and two free densification rates are needed. One set of experimental results, in which the stress free sintering rates for a body with high degree of anisotropy due to applied stress has been measured. It is shown that for this extreme case, the maximum value for the ratio of the anisotropic sintering strain rates is about 1.65.

Acknowledgements

This study used facilities established under the United States of America National Science Foundation Grants DMR 9257027 and DMR 9410981. We acknowledge funding by the Deutsche Forschungsgemeinschaft under Ro954/14 and thank Emil Aulbach for experimental support.

References

[1] Riedel H, Meyer D, Svoboda J, Zipse H. Int J Refract Met Hard Mater 1993–1994;12:55.
[2] Kim HG, Gillia O, Doremus P, Bouvard D. Int J Mech Sci 2002;44:2523.
[3] Scherer GW. J Non-Cryst Solids 1979;34:239.
[4] Scherer GW, Garino TJ. J Am Ceram Soc 1985;68:216.
[5] Mikeska KR, Scherer GW, Bordia RK. Ceram Trans 1990;7:200.
[6] Bordia RK, Scherer GW. Acta Metall 1988;36:2393.
[7] Bordia RK, Scherer GW. Acta Metall 1988;36:2399.
[8] Olevsky EA. Mater Sci Eng 1998;R23:41.
[9] Rahaman MN, De Jonghe LC. J Am Ceram Soc 1984;67:C205.
[10] Raj R, Bordia RK. Acta Metall 1984;32:1003.
[11] Venkatachari KR, Raj R. J Am Ceram Soc 1986;69:499.
[12] Cai PZ, Messing GL, Green DJ. J Am Ceram Soc 1997;80:445.
[13] Gillia O, Josserond C, Bouvard D. Acta Mater 2001;49:1413.
[14] Kim HG, Gillia O, Bouvard D. J Eur Ceram Soc 2003;23:1675.
[15] Zuo R, Aulbach E, Bordia RK, Rödel J. J Am Ceram Soc 2003;86:1099.
[16] Zuo R, Aulbach E, Rödel J. Acta Mater 2003;51:4563.
[17] McMeeking RM, Kuhn LT. Acta Metall Mater 1992;40:961.
[18] Du ZZ, Cocks ACF. Acta Metall Mater 1992;40:1969.
[19] Svoboda J, Riedel H. Acta Metall Mater 1992;40:2829.
[20] Zuo R, Aulbach E, Rödel J. J Am Ceram Soc 2004;87:526.
[21] Bordia RK, Jagota A. J Am Ceram Soc 1993;76:2475.
[22] Bordia RK, Raj R. J Am Ceram Soc 1985;68:287.
[23] Jagota A, Hui CY. Mech Mater 1991;11:221.
[24] Garino TJ, Bowen HK. J Am Ceram Soc 1990;73:251.
[25] Bang J, Lu GQ. J Mater Res 1995;10:1321.
[26] Choe JW, Calata JN, Lu GQ. J Mater Res 1995;10:986.
[27] Lu GQ, Sutterlin RC, Gupta TK. J Am Ceram Soc 1993;76:1907.
[28] Tzeng SY, Jean JH. J Am Ceram Soc 2002;85:335.
[29] Mikeska KR, Jensen RH. Ceram Trans 1990;15:629.
[30] Cai PZ, Green DL, Messing GL. J Am Ceram Soc 1997;80:1929.
[31] Zuo R, Aulbach E, Rödel J. J Mater Res 2003;18:2170.
[32] Flinn BD, Bordia RK, Zimmermann A, Rödel J. J Eur Ceram Soc 2000;20:2561.
[33] Salamone SM, Stearns LC, Bordia RK, Harmer MP. J Am Ceram Soc 2003;6:883.